CHAPTER 4

IMPLEMENTATION OF CYLINDRICAL MICROSTRIP PATCH ARRAYS

The null synthesis techniques proposed in the previous chapter do not consider the mutual coupling between the antenna elements and it is also assumed that the antenna elements do not disturb each other's current distributions. Each element's radiation pattern is thus considered to be identical to the radiation pattern of an isolated antenna in both shape and radiation strength. The input impedance of each antenna element is furthermore assumed to be matched to the impedance of its port in the feeding network.

These assumptions are valid when large inter-element spacings and low substrate heights are used to minimise the effects of the mutual coupling. In Chapter 3, it was seen that the utilisation of large inter-element spacings leads to wide nulls with high gain ripple in the omni-region. The use of a low substrate height is also not favoured since it decreases the realisable bandwidth. Small inter-element spacings and higher substrate heights are therefore preferred to yield null patterns with a reasonable bandwidth within the pattern specifications.

When small inter-element spacings are used, distortion of the excitations may occur due to the mutual coupling. The desired radiation pattern is consequently deteriorated due to the errors in the element excitations [72, 73]. During null synthesis, these erroneous

excitations lead to null filling and null position errors [53, 74]. The nulls introduced in the beam patterns of linear monopole arrays were found to be shifted or filled due to the mutual coupling [74]. Abele [54] studied the effect of the mutual coupling on the null pattern of a cylindrical dipole array and found that the coupling needed to be compensated for to prevent distortion of the null characteristics.

In this chapter, an investigation into the extent to which the mutual coupling has an influence on the null pattern of a cylindrical microstrip patch array will be done. When it is established that the mutual coupling may not be neglected for a specific array configuration and null pattern, a technique to compensate for the mutual coupling will be needed.

Yang *et al* [86] proposed a mutual coupling compensation technique to obtain the desired bandwidth and voltage standing wave ratio (VSWR) at the resonant frequency for an electromagnetically coupled (EMC) dipole antenna array. For a given set of excitation voltages, the dipole lengths and dipole offsets from the microstrip feed line were altered to obtain the prescribed driving admittances seen by the feed lines. As a result, a good similarity was also found between the desired and measured radiation patterns. Chen *et al* proposed a similar technique for a linear array of parallel dipoles [88]. The lengths and the radii of the dipoles were changed to obtain equal driving impedances for all the dipoles. Consequently, the desired radiation pattern was obtained. In this chapter, the mutual coupling compensation technique is applied to both linear and cylindrical microstrip patch arrays.

In the first section, the design of a cylindrical microstrip patch element for both polarisations will be discussed. The effect of the mutual coupling on the bandwidth of a linear microstrip patch array will be investigated firstly. This investigation was conducted in order to study the improvement in the bandwidth due to the use of the mutual coupling compensation technique. Afterwards, the effect of coupling on the array imbedded element pattern of the cylindrical microstrip patch element will be shown. The influence of the mutual coupling on the null pattern of a cylindrical microstrip patch will also be investigated for various inter-element spacings and both polarisations. The mutual coupling compensation technique will be used for both the linear and cylindrical microstrip patch arrays. The improvement in the characteristics of the linear and cylindrical patch arrays due to the compensation technique will be discussed using two test cases.

4.1 Design of cylindrical microstrip patch element

In the investigation of the cylindrical microstrip patch arrays, probe-fed microstrip patches were also utilised as the array elements. To assist with the design of the array elements, a commercial electromagnetic software package which apply the Finite Difference Time Domain (FDTD) method [101], was used. To verify the results of the software package, a single element was designed, manufactured and measured. The measured results were then compared with the simulated results.

Figure 4.1 illustrates the cylindrical microstrip patch element (axially polarised) on a copper cylinder, as well as the probe feeding mechanism. The patch element consisted of a 5mm layer of air, a thin layer of FR4 ($\varepsilon_r = 4.17$) and a 36 μm layer of copper. The patch was etched onto the thin layer of FR4 (with a thickness of 0.127mm) and conformally shaped to the patch along the surface of the cylinder.

The FDTD software package uses conforming cell elements in the xy-plane, and rectangular cell elements in the xz- and yz-planes. To make use of the conforming cells, the axes of the cylinder were thus aligned with the z-axis. The three main considerations during the design of the single element using the software, were the simulation of the probe feeding, the thin layer of copper and the thin layer of FR4.

When the thin layers of FR4 and copper were used in the simulation, a very large number of cells was generated during the meshing of the problem. This high number of cells exceeded the simulation capability of the software and an alternative method for the simulation of the problem was thus needed. The effect of the thin layer of FR4 was simulated by combining the layers of air and FR4 into one layer. The characteristics of the combined layer were found by simulating and comparing the input impedances of a planar patch with the two layers and a planar patch with a combined layer. A single layer with a height of 4.77mm and $\varepsilon_r = 1.0705$ were found to yield similar results compared to the double layer. The thickness of the copper layer was increased to 1mm in order to reduce the number of cells.

The probe-feed was simulated using a square co-axial probe. The dimensions of the probe-feed were designed for $S_{11} = S_{22} = 0$ and $S_{12} = S_{21} = 1$. The resulting centre conductor had a diameter of 0.8mm. The outer conductor had an outer diameter of 4mm and a thickness of 0.45mm. The dielectric material in the coax had an ε_r of 2.3.

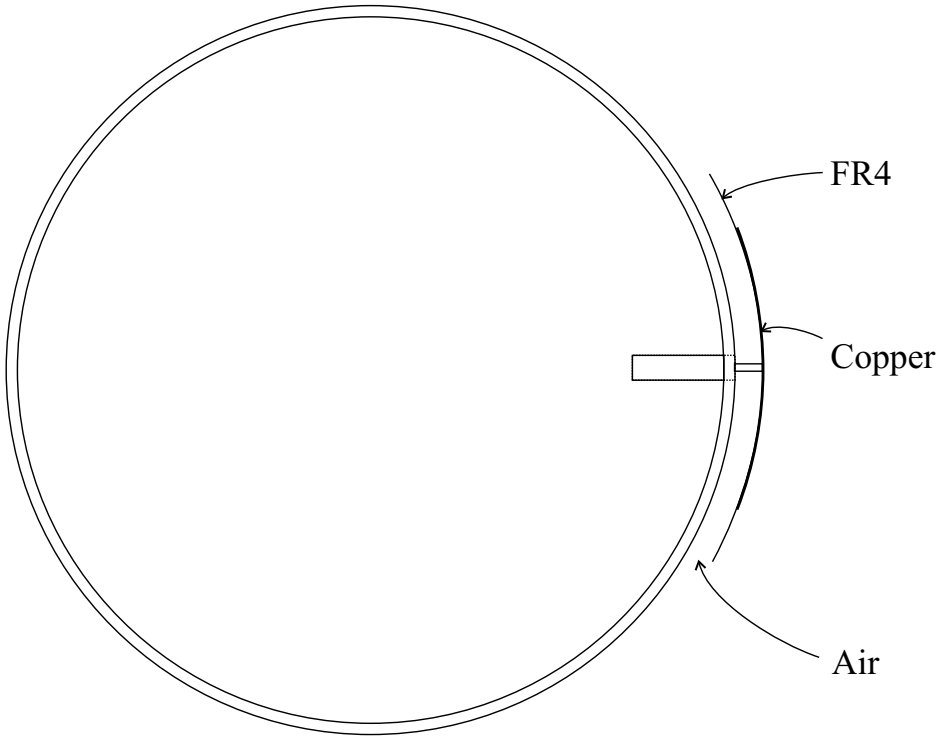

Figure 4.1: Top view of cylindrical microstrip patch on a copper cylinder with a radius of 127 mm and a thickness of 2 mm

The effects of the above approximations on the simulated results were studied by designing a single element and by comparing the simulated and measured results. A planar patch was designed for a resonant frequency of 1.8 GHz, with resulting dimensions of $L = 73.1$ mm, $W = 76$ mm and $y = 20.85$ mm. The planar patch was simulated with a copper thickness (t) of 0mm (using a perfectly conducting boundary) and 1mm. The same patch element was also used to form the axially polarised cylindrical patch element and was simulated with the above mentioned approximations. A 250mm high cylinder with $a = 127$ mm and $h = 2$ mm was used. Both the planar and cylindrical patch elements were manufactured and their reflection coefficients were measured.

Figure 4.2 compares the simulated and measured reflection coefficients for the planar and cylindrical patch elements. For the planar patch, the simulation yielded a lower resonant frequency (1.774 GHz) for $t = 0$ mm compared to the measured resonant frequency of 1.798 GHz. For the thicker layer of copper ($t = 1$ mm), the resonant frequency is even lower at 1.744 GHz. This decrease in the resonant frequency is due to the wider fringing fields. The simulation for the cylindrical patch with $t = 1$ mm yielded a resonant frequency of 1.735 GHz. In comparison, a higher resonant

frequency of 1.808GHz was obtained from the measurements of the cylindrical patch. The resonant frequencies of the measured planar and cylindrical patches differed by only 10 MHz.

The lower resonant frequency of the simulated reflection coefficient must thus be taken into account when designing the cylindrical patch element. The reflection coefficients of the simulated and measured cylindrical patch elements also differ by 7.7 dB, which must also be considered during the design.

The simulated and measured radiation patterns of the axially polarised patch element were also compared. The comparison of the patterns at the respective resonant frequencies can be seen in Figure 4.3. The radiation pattern was measured with the centre of the cylindrical patch pointing towards 0°. In the main beam region, between −100° and 100°, the patterns are very similar. At 180° the radiation patterns differ by 3.2 dB.

The effect of the approximations was also studied for a circumferentially polarised cylindrical patch element. The thin layer of FR4 and the 5mm layer of air were also combined into one layer and the copper patch had a thickness of 1mm in the simulations. The dimensions of the patch element were $L = 75$ mm and $W = 76$ mm. The feed position was at 16.9 mm in the ϕ-direction from the centre of the patch. The simulated and measured results for the reflection coefficients are compared in Figure 4.4. The resonant frequency of the measured results (1.779 GHz) was also higher than the resonant frequency (1.727 GHz) yielded by the simulation. The simulated and measured reflection coefficients at their respective resonant frequencies differed by 6.8 dB.

Figure 4.5 compares the measured and simulated radiation patterns for the circumferentially polarised patch. The two patterns compared well in the main beam region between −60° and 60°, but differ slightly outside this angular range.

The above shifts in the resonant frequencies and changes in the input impedances can consequently be applied to refine the design of the axially and circumferentially polarised patch elements for the desired resonant frequency and input impedance. Manufacturing tolerances will however still have an influence on the measured results.

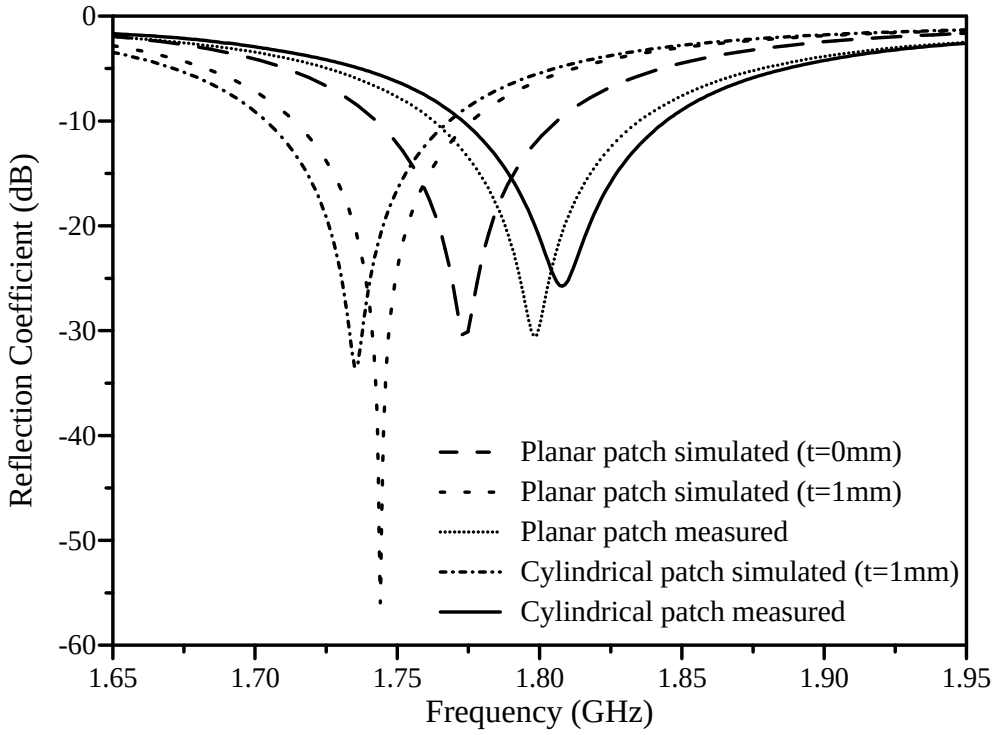

Figure 4.2: Simulated and measured reflection coefficients for planar and cylindrical patch (axially polarised) elements

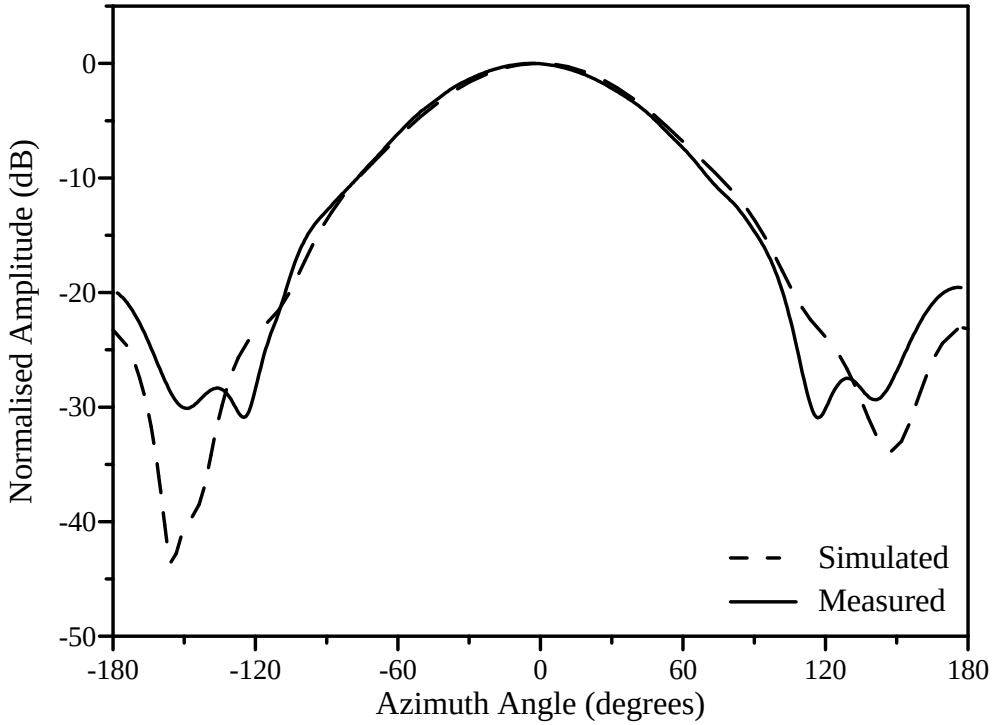

Figure 4.3: Simulated and measured radiation patterns for the axially polarised patch element

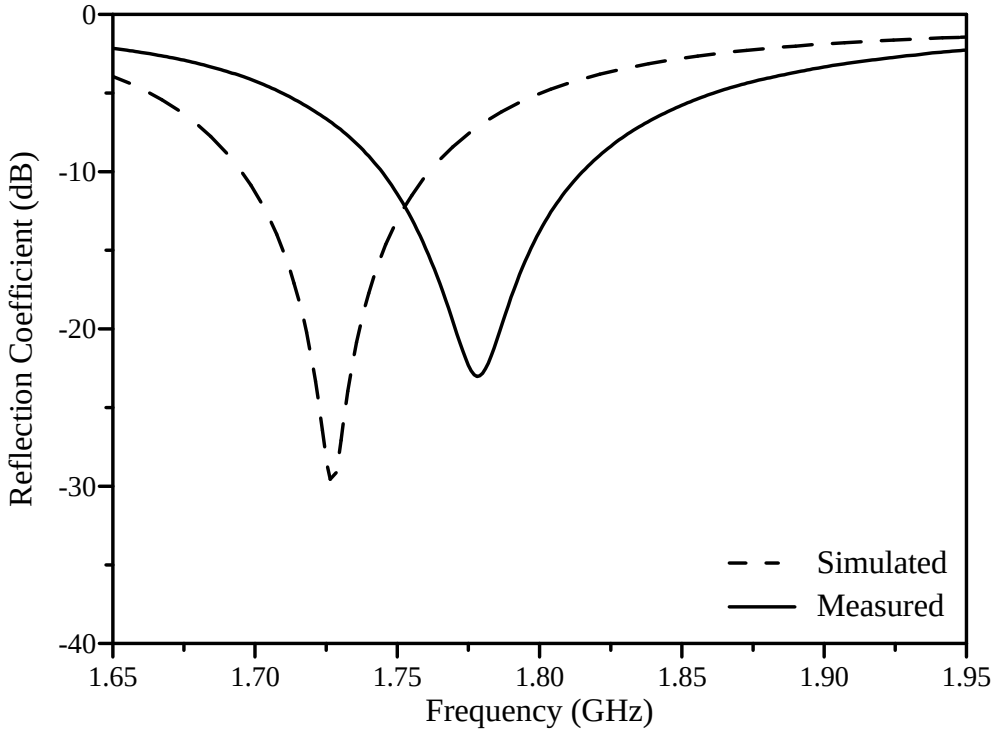

Figure 4.4: Simulated and measured reflection coefficients for the circumferentially polarised patch element

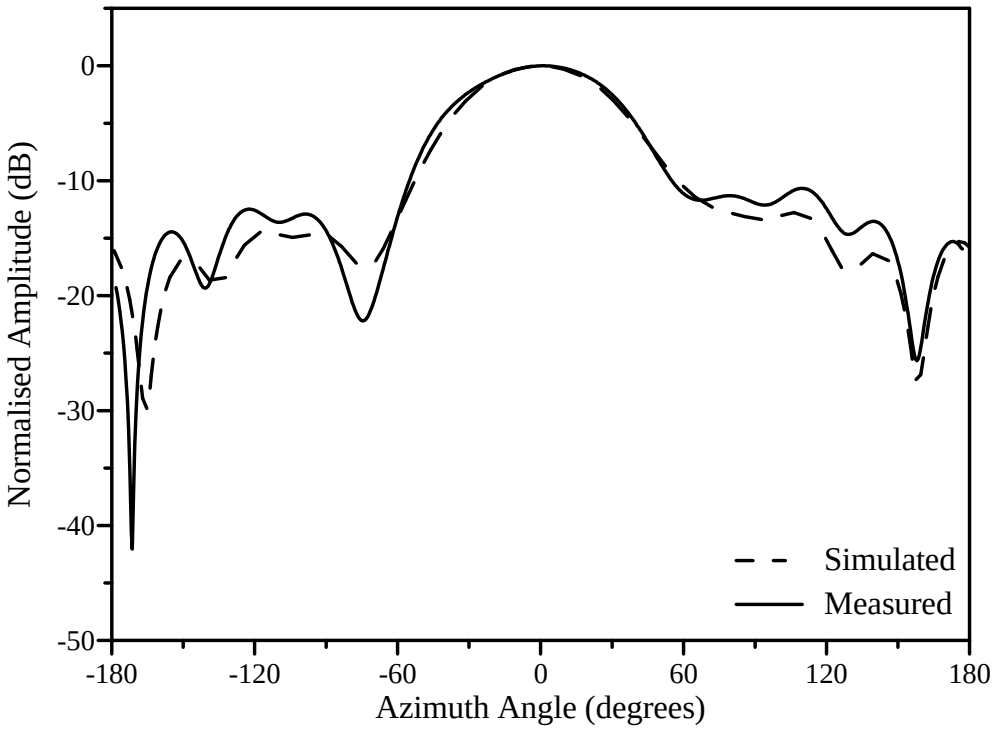

Figure 4.5: Simulated and measured radiation patterns for the circumferentially polarised patch element

4.2 Effect of mutual coupling

4.2.1 Effect of mutual coupling for linear patch arrays

The effect of the mutual coupling on the bandwidth and resonant frequency of a linear microstrip patch array was investigated. The investigation was done for specific array configurations and co-operate feed networks were used to excite the elements. The results of this investigation will be used to study the improvement in the bandwidth and resonant frequency of a linear patch array when a mutual coupling compensation technique is used, which will be discussed later in this chapter.

Probe-fed microstrip patch antennas are considered as narrowband antenna elements with bandwidths smaller than 5% for a voltage standing wave ratio (VSWR) of 1.5. Bandwidth enlargement may be obtained by increasing the height of the patch antenna, which on the other hand leads to an increase in the inductive reactance of the probe. The high reactance prevents the matching of the antenna element's input impedance by varying only the remaining physical parameters of the antenna.

Due to the narrowband nature of the elements, mutual coupling may significantly degrade the performance of an array. For linear arrays two types of mutual coupling are defined [62]. E-plane coupling refers to the mutual coupling existing between end coupled patches forming a linear array in the E-plane of the antenna radiation. The coupling between parallel coupled patches, forming a linear array in the H-plane of the antenna radiation, is referred to as H-plane coupling.

To investigate the influence of the E-plane mutual coupling, a uniform four element linear microstrip patch array as shown in Figure 4.6 was used. Without any mutual coupling compensation, the probe-fed microstrip patch antenna elements were designed for a resonant frequency of 1.8 GHz. For a single isolated patch a simulated bandwidth of 2.9% for a VSWR of 1.5 was obtained with 5mm air and 1.6mm dielectric substrate with $\varepsilon_r = 4.4$. L_n, W_n and y_n in Figure 4.6 were 62.8mm, 65mm and 12.9mm for all n, respectively. A simple cooperate feed network with 50Ω ports was designed to excite the four patches with equal amplitude and phase. Only 50Ω microstrip lines were used in the cooperate feed network.

Four identical patches were used to form arrays with different inter-element spacings, d, to study the effect of the mutual coupling on the reflection coefficient. The simulated

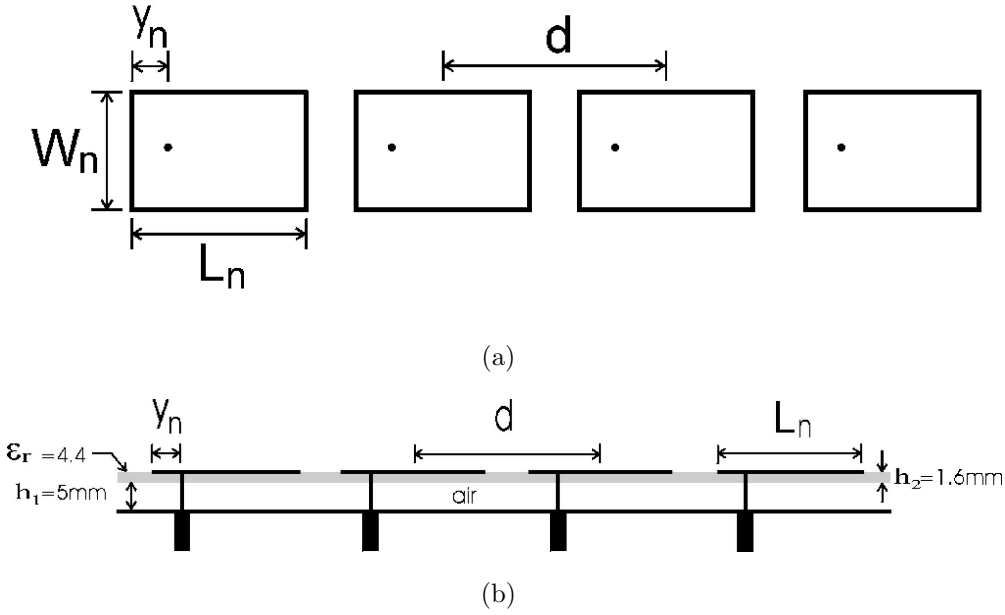

Figure 4.6: Four element linear microstrip patch array: (a) Top view, (b) Side view

reflection coefficients at the input ports of the feeding networks for the arrays with different inter-element spacings are shown in Figure 4.7. It is seen that both the minimum of the reflection coefficient and the resonant frequency are influenced by the mutual coupling. For $d = 0.5\lambda_0$, the resonant frequency shifted by 2.8%, which is close to the bandwidth of an isolated patch. In this case, there is also no measurable bandwidth for a VSWR of 1.5. As the inter-element spacing increases, the coupling between the antenna elements decreases and has less effect on the bandwidth and resonant frequency. Table 4.1 summarises the magnitude of the E-plane coupling and the resulting characteristics for the different inter-element spacings. The tabulated coupling is the coupling between two neighbouring patch antennae.

The effect of H-plane mutual coupling was also studied by rotating the four antenna elements individually by 90°. Figure 4.8 compares the simulated reflection coefficients at the input ports of the feeding networks for arrays with different inter-element spacings. Due to the smaller magnitude of the H-plane coupling, the resonant frequency and bandwidth are less influenced. The bandwidth of the array with an inter-element spacing of $d = 0.5\lambda_0$ decreased by 0.7% to 2.2%. The coupling magnitude and the resulting characteristics are also summarised in Table 4.1.

It is evident that the characteristics of these narrowband arrays are effected by the mutual coupling. A high coupling factor can alter the resonant frequency to such an

extent that the active bandwidth of the array falls outside the desired bandwidth. The bandwidth at a VSWR of 1.5 decreases as the mutual coupling increases. An increasing coupling also causes the minimum reflection coefficient at the resonant frequency to increase. A technique is thus needed to match the desired and active characteristics.

Table 4.1: Characteristics at the input port of a linear microstrip patch arrays

Coupling	**Spacing** (λ_0)	**Coupling factor (dB)**	**Resonant frequency (GHz)**	**Reflection coefficient (dB)**	**Bandwidth** (%)
E-plane	0.5	-10.4	1.748	-13.9	0.00
	0.6	-17.3	1.785	-16.0	2.13
	0.7	-23.4	1.800	-18.9	2.73
	0.8	-28.2	1.804	-23.3	2.94
H-plane	0.5	-16.2	1.800	-16.5	2.20
	0.6	-21.3	1.805	-18.6	2.77
	0.7	-25.1	1.809	-22.7	2.99
	0.8	-27.9	1.809	-30.7	2.99

4.2.2 Effect of mutual coupling on the amplitude pattern of cylindrical patch arrays

Similar to the planar microstrip patch arrays, the coupling between two cylindrical patches is referred to as either E-plane or H-plane coupling depending on the orientation of the patches [66]. For axially polarised patch arrays, the coupling is called H-plane coupling. E-plane coupling exists between two circumferentially polarised patches.

The coupling in an array has an effect on both the array imbedded radiation pattern of the element as well as the element excitations [17, 19, 72]. To illustrate the effect of the coupling on the array imbedded element pattern, an axially polarised patch array was manufactured on a cylinder with $a = 127$ mm and $h = 2$ mm. The array had 10 elements with an inter-element spacing of $d_\phi = 0.5\lambda_0$. The axially polarised patch element had dimensions of $L = 73.1$ mm and $W = 76$ mm. The feed position was 20.85 mm in the z-direction from the bottom of the patch element.

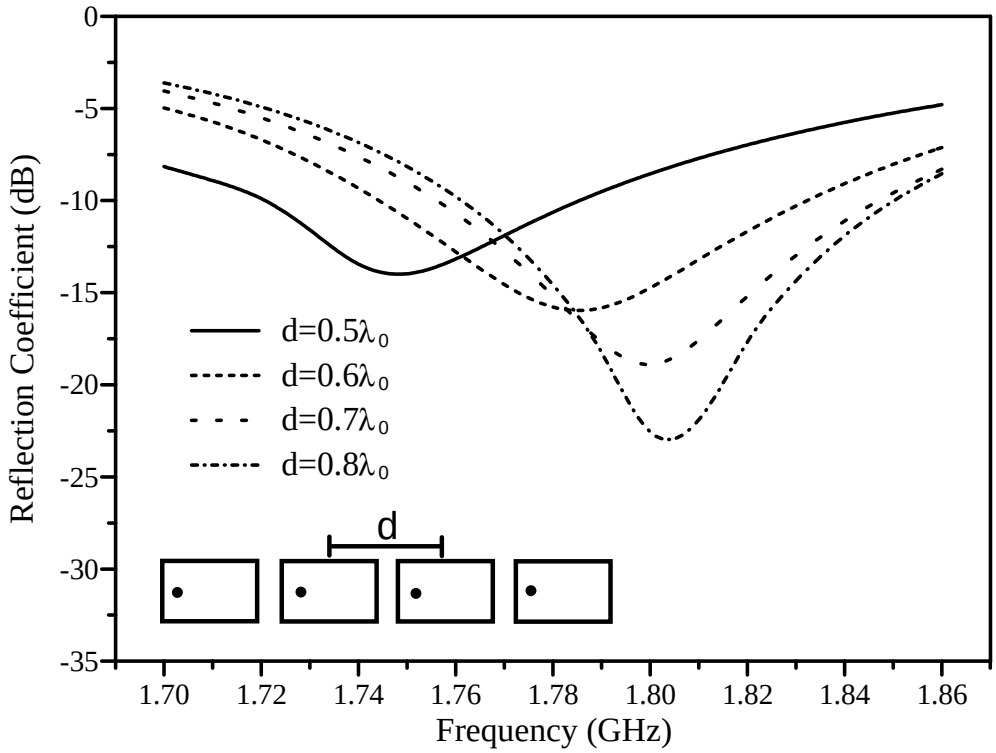

Figure 4.7: Simulated reflection coefficient at the feeding network input port of a horisontal polarised array (E-plane coupling) for different inter-element spacings

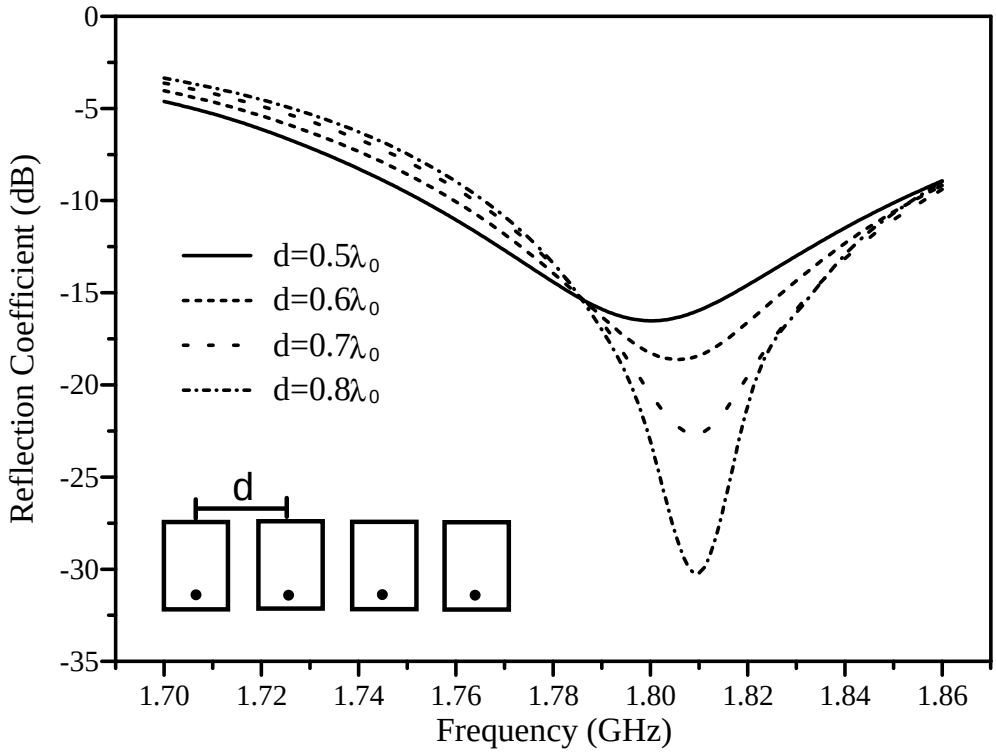

Figure 4.8: Simulated reflection coefficient at the feeding network input port of a vertically polarised array (H-plane coupling) for different inter-element spacings

The array imbedded element pattern was measured by exciting only one element while terminating the remaining elements with 50Ω loads. The same procedure was followed for the simulation of the active pattern. Figure 4.9 compares the measured and simulated active element radiation patterns with the radiation pattern of a single element. The simulated and measured patterns compare well within the region of the main beam and differ slightly in the region of the back lobe.

It is evident that the main beam of the element pattern is broader due to the mutual coupling between the patch elements. To prevent distortion of the resulting array pattern, it is thus important to use the active element pattern when determining the excitation coefficients for a specified array radiation pattern.

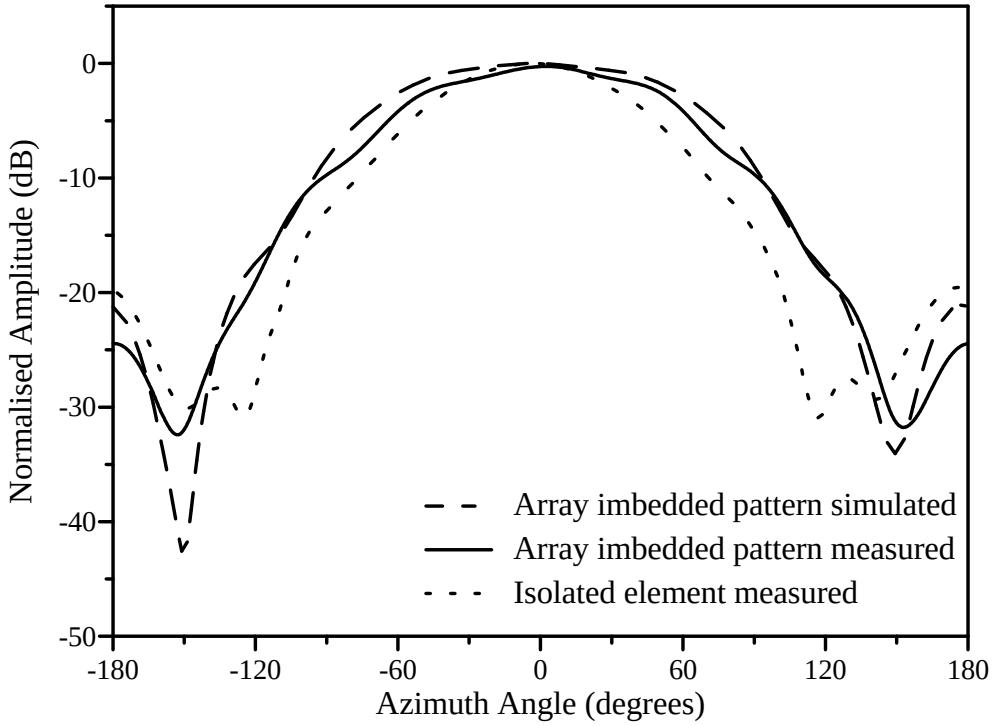

Figure 4.9: Simulated and measured array imbedded radiation patterns of an axially polarised patch in a cylindrical array with $d_\phi = 0.5\lambda_0$

The effect of the mutual coupling on a desired null pattern was also studied. A cylindrical patch array of 10 elements was simulated to study the influence of the mutual coupling on an omnidirectional radiation pattern with a single null. The same substrates as those used in the previous study, were used to form the patch elements. For both the axial and circumferential polarisations, the patch dimensions were $L = 73.1$ mm and $W = 76$ mm. The position of the feed was 15.7 mm in the z-direction from

the centre of the patch for the axial polarisation. For the circumferential polarisation, the feed was at 15.7 mm in the ϕ-direction from the centre of the patch.

The desired element excitations to form a null, with a null depth of 20 dB at 180°, were obtained from the constrained optimisation method. The gain ripple in the omni-region was constrained to 1 dB and no constraint was placed on the -10 dB null width. The element excitations for both polarisations were calculated without considering mutual coupling. Afterwards, the active driving currents were computed using the simulated admittance matrix in Equation 2.79 to study the influence of the mutual coupling on the null pattern. The array imbedded patterns of the axially and circumferentially polarised patches at their respective resonant frequencies of 1.735 GHz and 1.765 GHz, were used.

The simulated results for a circumferentially polarised patch array with an inter-element spacing of $0.5\lambda_0$ are shown in Figure 4.10. The resulting null pattern when there is no mutual coupling is compared with the resulting null pattern due to the active driving currents when mutual coupling is present. It can be seen that the mutual coupling increased the ripple and null width, while decreasing the maximum suppression of 20 dB to 16.7 dB. The position of the null was also changed by 3.25°, which consequently decreased the suppression at 180° by 4.36 dB. For this array configuration, Table 4.2 compares the normalised driving currents when there is no mutual coupling to the normalised active driving currents when mutual coupling is present.

Table 4.2: Influence of the mutual coupling on the driving currents for a circumferentially polarised patch array with $d_\phi = 0.5\lambda_0$ and $N = 10$

Element	**No Coupling**	**With Coupling**
1	$0.84\angle 4.19°$	$0.91\angle -25.07°$
2	$0.65\angle -73.20°$	$0.89\angle -41.09°$
3	$1.00\angle -22.09°$	$0.97\angle -60.70°$
4	$0.77\angle -78.80°$	$0.79\angle -82.15°$
5	$0.16\angle 63.21°$	$0.14\angle -2.31°$
6	$0.98\angle 68.67°$	$0.87\angle 54.78°$
7	$0.81\angle 89.29°$	$1.00\angle 43.57°$
8	$0.77\angle 48.62°$	$0.97\angle 23.16°$
9	$0.78\angle 44.89°$	$0.93\angle 8.94°$
10	$0.76\angle 23.36°$	$0.91\angle -8.32°$

Figure 4.11 shows the simulated patterns for a circumferentially polarised patch array with an inter-element spacing of $0.65\lambda_0$. For this larger inter-element spacing, the mutual coupling was smaller and the most significant observed change was in the ripple in the omni-region of the null pattern. For this case, the ripple increased from 1 dB to 2.86 dB, when the active element excitations are used. The results for the different inter-element spacings are summarised in Table 4.3 and Table 4.4. The coupling coefficients in these tables are the mutual coupling between an element and its nearest neighbour.

For the axially polarised patch array with an inter-element spacing of $0.5\lambda_0$, the results are shown in Figure 4.12. The resulting null pattern when there is no mutual coupling is compared with the resulting null pattern due to the active driving currents when mutual coupling is present. Both the ripple and null width were increased by the mutual coupling, while the maximum suppression was decreased by 1.46 dB. Table 4.5 compares the normalised driving currents when there is no mutual coupling to the normalised active driving currents when mutual coupling is present.

Figure 4.13 shows the resulting patterns for this array with an inter-element spacing of $0.65\lambda_0$. Although the mutual coupling is less for this larger inter-element spacing, the distortion of null pattern is more significant. In this case, the ripple and maximum suppression changed by 2.55 dB and 4.06 dB, respectively. Table 4.6 and Table 4.7 summarises the results for the different inter-element spacings.

The desired radiation pattern could not be obtained for inter-element spacings larger than $0.7\lambda_0$ and $0.65\lambda_0$ for the circumferentially and axially polarised arrays, respectively. This is due to the high ripple in the omnidirectional radiation pattern when large inter-element spacings are utilised.

Greater changes in the null positions and null widths are observed for the circumferentially polarised patch array. The change in the suppression at 180° and the change in the maximum suppression decreases as the spacing increases and the mutual coupling decreases for $d_\phi \leq 0.65\lambda_0$. For the larger inter-element spacing, as seen for $d_\phi = 0.7\lambda_0$, the element excitations tend to be more sensitive to the mutual coupling, although it is less than -20 dB. For the axial polarisation, the change in the suppression at 180° increases although the coupling decreases. For this polarisation, the increasing inter-element spacing thus makes the element excitations more sensitive to the mutual coupling.

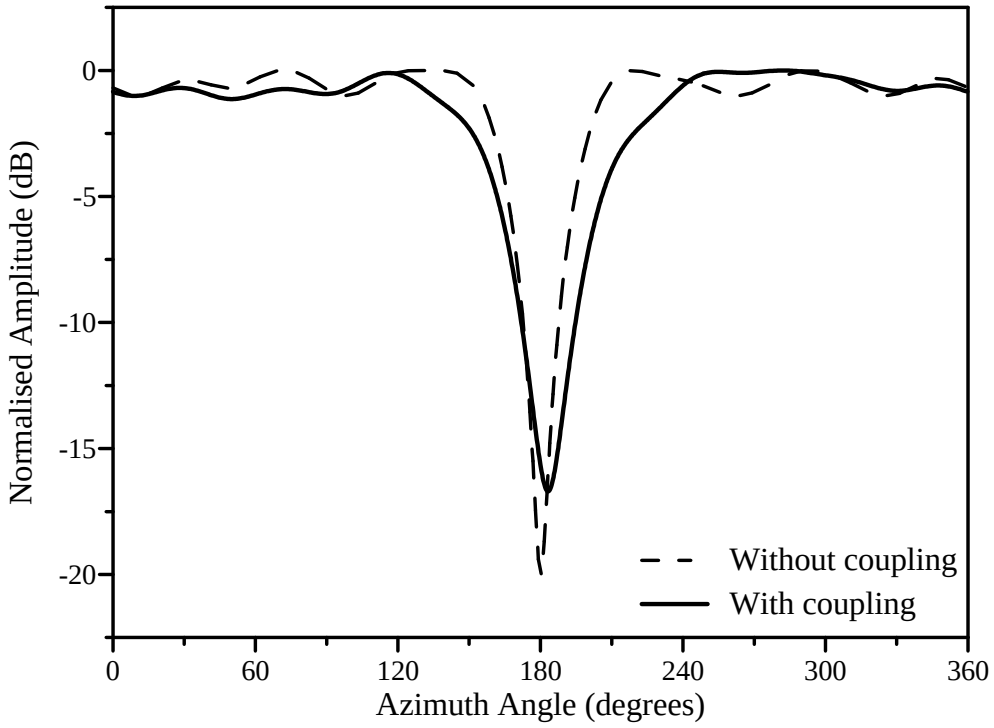

Figure 4.10: Normalised amplitude patterns of a circumferentially polarised patch array with $d_\phi = 0.5\lambda_0$ and $N = 10$

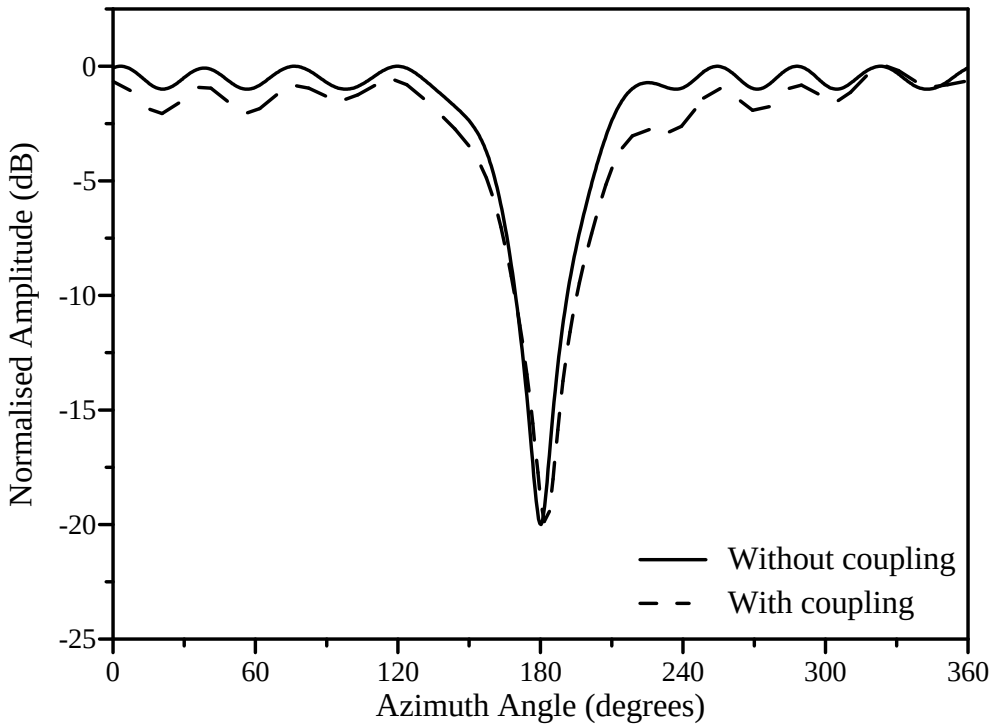

Figure 4.11: Normalised amplitude patterns of a circumferentially polarised patch array with $d_\phi = 0.65\lambda_0$ and $N = 10$

Table 4.3: Influence of the mutual coupling on the desired null pattern for a circumferentially polarised patch array

Spacing (λ_0)	**Coupling (dB)**	**Change in suppression at** 180° **(dB)**	**Change in maximum suppression (dB)**
0.5	-10.7	4.36	3.3
0.55	-13.3	4.23	1.95
0.6	-16.1	1.37	0.05
0.65	-18.8	1.21	-0.01
0.7	-21.1	4.3	3.52

Table 4.4: Influence of the mutual coupling on the desired null pattern for a circumferentially polarised patch array (continued)

Spacing (λ_0)	**Change in ripple (dB)**	**Change in null position (deg)**	**Change in null width (deg)**
0.5	0.14	3.25	7.80
0.55	0.40	4	7.69
0.6	1.51	2.25	6.69
0.65	1.86	2.25	4.34
0.7	4.63	2	-3.45

The inter-element spacing thus plays an important role in the choice of an array configuration. For small inter-element spacings in a circumferentially polarised array, the larger coupling between the elements has a greater influence on the radiation pattern. On the other hand, the use of large inter-element spacings makes the desired element excitations more sensitive to the mutual coupling for both polarisations. The coupling between axially polarised patches is smaller and the radiation pattern is less effected for small inter-element spacing.

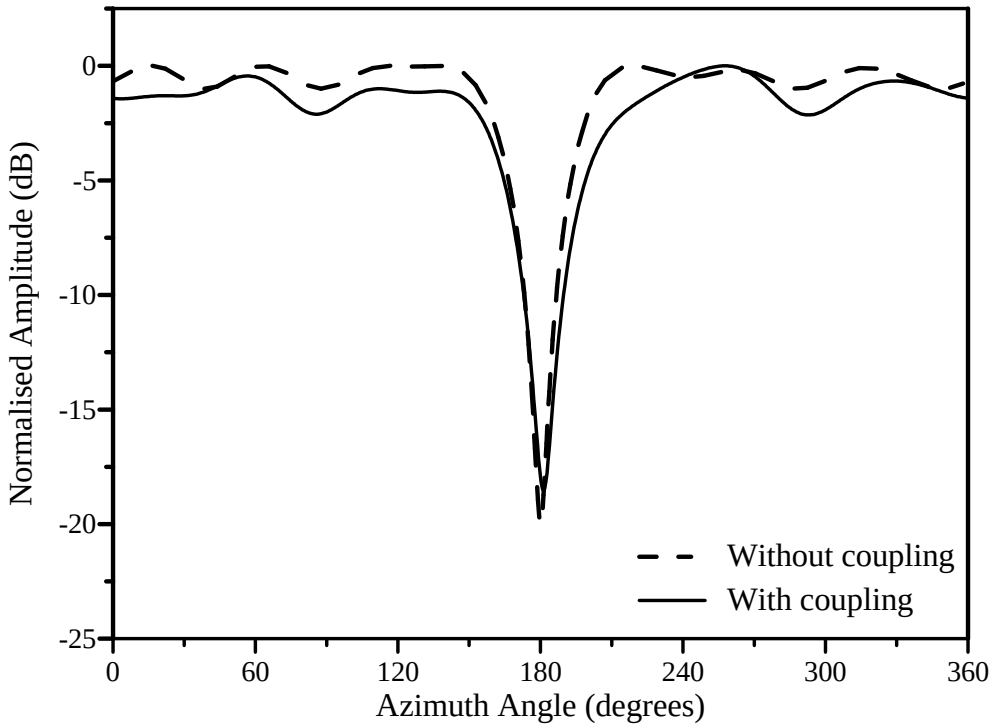

Figure 4.12: Normalised amplitude patterns of an axially polarised patch array with $d_\phi = 0.5\lambda_0$ and $N = 10$

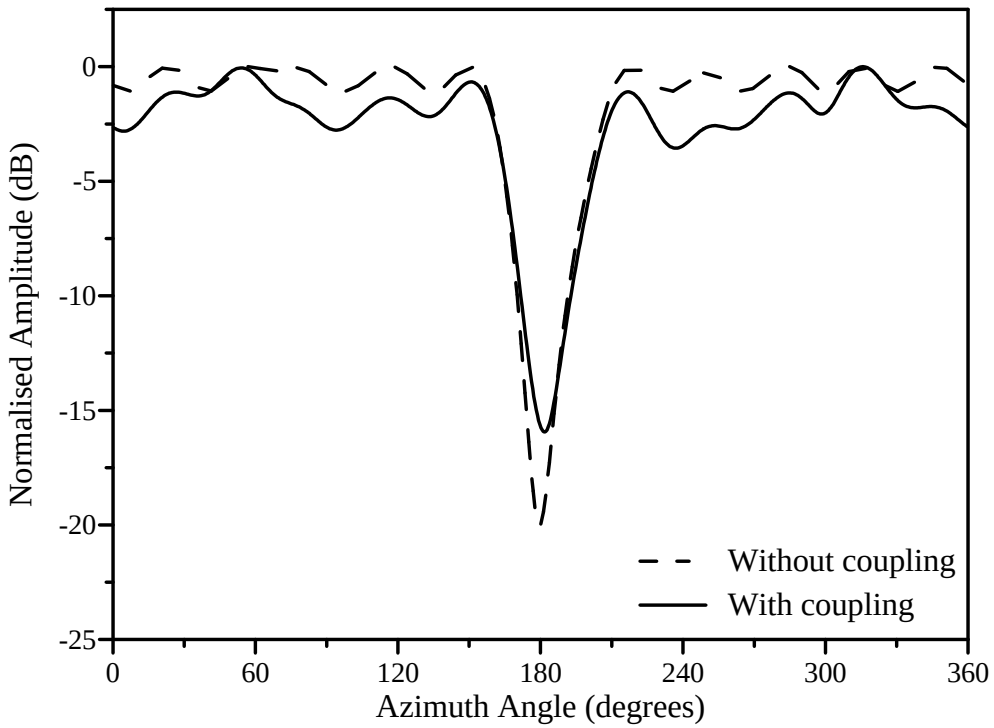

Figure 4.13: Normalised amplitude patterns of an axially polarised patch array with $d_\phi = 0.65\lambda_0$ and $N = 10$

Table 4.5: Influence of the mutual coupling on the driving currents for a axially polarised patch array with $d_\phi = 0.5\lambda_0$ and $N = 10$

Element	**No Coupling**	**With Coupling**
1	$0.79\angle 12.14°$	$0.81\angle -5.27°$
2	$0.70\angle -6.55°$	$0.84\angle -22.51°$
3	$0.95\angle -16.17°$	$0.84\angle -35.48°$
4	$0.75\angle -71.78°$	$0.79\angle -73.28°$
5	$0.18\angle 62.69°$	$0.13\angle 58.73°$
6	$1.00\angle 78.36°$	$1.00\angle 72.14°$
7	$0.73\angle 91.40°$	$0.76\angle 60.52°$
8	$0.81\angle 59.14°$	$0.92\angle 47.32°$
9	$0.76\angle 45.93°$	$0.77\angle 28.57°$
10	$0.77\angle 28.71°$	$0.88\angle 12.09°$

Table 4.6: Influence of the mutual coupling on the desired null pattern for a axially polarised patch array

Spacing (λ_0)	**Coupling (dB)**	**Change in suppression at** $180°$ **(dB)**	**Change in maximum suppression (dB)**
0.5	-17.6	2.08	1.46
0.55	-20.1	2.67	2.08
0.6	-22.5	2.67	1.83
0.65	-24.3	4.31	4.06

From Table 4.3 and Table 4.4, it is observed that for small inter-element spacing in the circumferential polarisation, the mutual coupling must be compensated for in order to obtain the desired radiation pattern. The compensation is also needed to correct the degree of suppression in a specified direction for all inter-element spacings and both polarisations.

Table 4.7: Influence of the mutual coupling on the desired null pattern for a axially polarised patch array (continued)

Spacing (λ_0)	**Change in ripple (dB)**	**Change in null position (deg)**	**Change in null width (deg)**
0.5	1.14	1.25	3.28
0.55	1.47	1	1.22
0.6	1.47	1.75	0.08
0.65	2.55	1.75	-0.23

4.3 Mutual coupling compensation

4.3.1 Mutual coupling compensation for linear patch arrays

Paragraph 2.4.3 discusses a technique in which the geometries of the elements are varied to provide matched and equal driving impedances for all the antenna elements, given a required set of element excitations. From Equation 2.80, the driving impedances may be written as:

$$Z_m^a = Z_{mm}^s(L_m, y_m) + \sum_{\substack{n=1 \\ n \neq m}}^{N} Z_{mn}(L_n, L_m, y_n, y_m)\frac{I_n}{I_m}, \tag{4.1}$$

where L_m and y_m are the length and feed position of the m-th patch antenna element, respectively. The length and feed position of the n-th neighbouring antenna element are represented by L_n and y_n, respectively. Both the self impedance and mutual impedances are expressed as functions of the length and feed positions. Although the above impedances also vary with the widths and heights of the patch antennae, these dimensions are kept constant to reduce the dimensionality of variable space.

A commercial electromagnetic software package [100] which utilises the method of moments, is used to obtain Z_{mm}^s and Z_{mn} for different lengths and feed positions. For the linear array configuration in Figure 4.6, Z_{mn} has a low sensitivity to small variations in the feed positions and the dimensionality of Z_{mn} can thus be even further reduced. The self and mutual impedances are computed for linearly spaced values

of the lengths and feed positions and are placed in two lookup tables. One lookup table is populated with the self impedance values with respect to the lengths and feed-positions of a single antenna element. Another lookup table is populated with the mutual impedance values with respect to the lengths of two neighbouring antenna elements. A least squares optimisation algorithm is used to determine the lengths and feed positions at which the driving impedances of all the patches are equal to 50Ω. N lengths and N feed positions are used as the variables and the algorithm interpolates between the computed impedance values using a bicubic spline algorithm. For each antenna element an error in the real part of impedance as well as an error in the imaginary part of the impedance is calculated. The cost function is then determined as the sum of the $2N$ squared errors. The least squares optimisation algorithm determines the N lengths and N feed positions which minimise this cost function.

An example in which the mutual compensation technique is applied to a linear patch array, is incorporated into the test case in paragraph 4.4.1.

4.3.2 Mutual coupling compensation for cylindrical arrays

The mutual coupling compensation technique described in paragraph 4.3.1 for the linear patch array will also be used for the cylindrical patch arrays. For the cylindrical arrays, L_m and y_m in equation 4.1 are respectively the length and feed position of the m-th patch element along the direction of its polarisation.

The look-up table, which is used to search for the necessary lengths and feed positions to adjust the active driving impedances to 50Ω, is populated using simulation results from the FDTD software.

As an example, the lengths and feed positions were found to correct the null pattern in Figure 4.10 for the axially polarised array with $d_\phi = 0.5\lambda_0$ and $N = 10$. The starting values used by the optimisation algorithm for all n elements, were L_n=73.1 mm and y_n=20.85 mm. A graphical representation of the variable space for the self-impedance is shown on a Smith chart in Figure 4.14. The variable space is shown for 71.6mm $\leq L_n \leq$ 74.6mm and 4.85mm $\leq y_n \leq$ 26.85mm. During the search for the appropriate lengths and feed positions, it was assumed that small changes in the lengths and feed positions, do not have a significant effect on the mutual coupling and was considered to stay constant. The resulting lengths and feed positions needed to

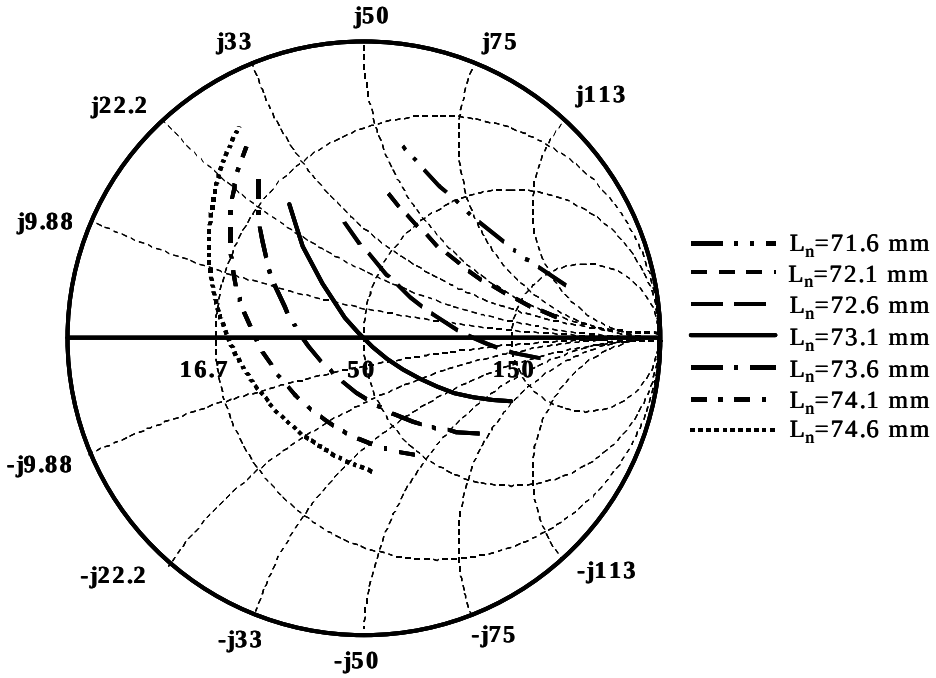

Figure 4.14: Self-impedance of the axially polarised patch antenna element for different L_n and $4.85mm \leq y_n \leq 26.85mm$

correct the element driving impedances for the desired set of excitations, are listed in Table 4.8.

The above procedure was also repeated for the sets of element excitations obtained for the circumferentially polarised patch arrays and the remaining axially polarised arrays. A self-impedance look-up table was set up for the patch antenna element of each array configuration.

The optimisation algorithm was then used to search for the lengths and feed positions to correct the active driving impedances and consequently the desired null pattern for each array.

For the circumferential polarisation and inter-element spacing of $0.5\lambda_0$, $0.55\lambda_0$ and $0.6\lambda_0$, the active driving impedance of the element in the same direction as the null could not be set to 50Ω. The simulated active driving impedances due to the desired set of excitations for the circumferentially polarised array with $d_\phi = 0.55\lambda_0$, is listed in Table 4.9. The active driving impedances for the desired set of excitations of the axially polarised array with $d_\phi = 0.55\lambda_0$, are also shown for comparison.

Table 4.8: Lengths and feed positions needed to correct the active driving impedances of an axially polarised patch array with $d_\phi = 0.5\lambda_0$

Element	**Length (mm)**	**Feed-position (mm)**
1	73.3	23.45
2	73.4	25.00
3	73.5	23.05
4	72.8	21.30
5	73.6	25.10
6	73.0	22.60
7	73.6	26.10
8	73.1	22.85
9	73.4	24.00
10	73.1	22.85

Table 4.9: Comparison of the active driving impedances for the desired null patterns of the circumferentially and axially polarised patch arrays with $d_\phi = 0.55\lambda_0$

Element	**Circumferential polarisation**	**Axial polarisation**
1	39.4 + j11.3	46.2 + j17.2
2	13.3 + j20.6	46.5 + j13.4
3	50.6 + j15.8	51.2 + j9.90
4	31.7 - j6.30	43.3 + j4.70
5	71.6 + j78.5	49.4 + j24.0
6	35.9 - j1.40	45.7 + j9.10
7	40.1 + j38.3	51.4 + j17.4
8	30.8 - j1.50	42.2 + j11.2
9	34.6 + j26.5	42.2 + j15.4
10	28.2 + j11.4	43.7 + j9.80

For the axially polarised array, with mutual coupling of -20.1 dB between nearest neighbouring elements, the desired input impedance could be found for all 10 elements within the available range of self-impedances. On the other hand, the higher mutual coupling (-13.3 dB) of the circumferentially polarised array contributed to a higher reactance of the driving impedance of the 5th element, which is in the same direction as the null. Consequently, the desired input impedance for this element could not be found within the range of input impedances for the specified patch antenna element configuration. The active driving impedance of this element could therefore not be modified to be exactly 50Ω and the effect of the mutual coupling could not be completely compensated for.

The mutual coupling thus places a constraint on the set of element excitations for which the mutual coupling can be compensated for, using the described compensation technique. This set of element excitations is determined for the desired null pattern and therefore the specifiable characteristics of the null pattern is limited.

A study was therefore conducted to determine the possible null depths of a single null for which the mutual coupling can be compensated for using the specified compensation technique. The element excitation sets for null patterns with various null depths were determined for the circumferentially and axially polarised patch arrays studied in the previous sections. For each specified null depth, it was determined if the desired self-impedances could be found within the available range of self-impedances to compensate for the mutual coupling.

The resulting possible null depths are summarised in Table 4.10 for both polarisations. The study was only conducted for suppression levels up to 40 dB. For all the axially polarised patch arrays with null patterns having null depths of up to 40 dB, the mutual coupling could be compensated for using the described compensation technique. On the other hand, the possible null depths for the null patterns of the circumferentially polarised patch arrays were limited to the values listed in Table 4.10. For null depths larger then the listed values, the mutual coupling could not be compensated for.

For high suppression levels and small inter-element spacing, the mutual coupling in the axially polarised array could be compensated for by using the described mutual coupling compensation technique. On the other hand, the realisable suppression levels were smaller for the circumferential polarisation when the mutual coupling was compensated for using the compensation technique.

Table 4.10: Comparison of possible null depths for circumferentially and axially polarised patch arrays with N=10

Spacing (d_ϕ) (λ_0)	**Circumferential polarisation**	**Axial polarisation**
0.5	-10 dB	-40 dB
0.55	-15 dB	-40 dB
0.6	-15 dB	-40 dB
0.65	-25 dB	-40 dB

4.4 Test cases

4.4.1 Linear patch array test case

A four element microstrip patch array with E-plane coupling was chosen to confirm experimentally the proposed coupling compensation technique. Initially, L_n, W_n and y_n in Figure 4.6 were 62.8mm, 65mm and 12.9mm for all n, respectively. The inter-element spacing was $d = 0.65\lambda_0$ and the self and mutual impedances of the array were computed for different lengths and feed positions using L_n=62.8mm and y_n=12.9mm as the centre variable values of the look-up tables.

A graphical presentation of the variable space for the self impedance is shown on a Smith chart in Figure 4.15. Each impedance curve is formed by keeping L_n constant and varying y_n between 8.9mm and 15.9mm. The optimisation algorithm is constrained to search only within this available self impedance space.

Careful attention should be paid to the element radiation pattern when setting up the look-up tables and variable space. Significant changes in the radiation pattern of the element should be avoided to prevent distortion of the total array radiation pattern. When the probe feed is put too close to the edge of the patch, the probe radiation may alter the element radiation pattern. If the length of the patch is varied too much, the beamwidth of the main beam in the element radiation pattern will be modified. The extent of these effects will vary between patch antenna element configurations.

The optimisation algorithm uses L_n=62.8mm and y_n=12.9mm as the starting values for all n elements to search for the lengths and feed positions where the driving impedances of all the patches are 50Ω. The resulting lengths are: L_1=L_4=63.2mm, $y1$=$y4$=11mm,

L_2=L_3=63.7mm and $y2$=$y3$=8.9mm. Using these parameters, the corresponding self impendances are: Z^s_{11}=Z^s_{44}=48.72-j7.87 and Z^s_{22}=Z^s_{33}=45.08-j14.11.

To verify the simulation results with measurements, both arrays were built and simple cooperate feed networks were designed to excite all patch antennas with equal amplitude and phase. The feed networks consisted of only 50Ω microstrip lines. The S-parameters of both arrays were measured and used in the simulation software to compute the reflection coefficients at the input ports of the feed networks of the arrays. The narrowband arrays built for the measurements were influenced by uncertainties in certain parameters such as the height of the air region, the permittivity of the substrate at high frequencies and some reactance added by the coaxial probes. To compensate for these uncertainties, a single isolated patch was used as a test case, and had to be slightly altered to get good correspondence between simulated and measured results for the single patch. The width had to be increased by 4mm and a width of W_n=69mm was subsequently used for all the patches of both experimental arrays.

Figure 4.16 compares the simulated and measured results for the original uncompensated and compensated arrays. The top views of the uncompensated and compensated arrays are shown in Figures 4.17 and 4.18, respectively. The side view of the compensated array is shown in Figure 4.19. The results show good similarity between the simulated and measured reflection coefficients and the improvement due to compensation technique is clearly visible. The resonant frequency of the compensated array is within 0.1% of 1.8GHz and the measured bandwidth for a VSWR of 1.5 increased from 2.3% to 3.9%, which is an improvement of 69.6% in bandwidth. The measured reflection coefficient at 1.8GHz improved from -17.3dB to -32dB. The technique is thus able to correct the individual driving impedances of the antenna elements and thereby improve the reflection coefficient at the input port of the array feed network.

4.4.2 Cylindrical patch array test case

An axially polarised patch array with N=10 and $d_\phi = 0.5\lambda_0$ was chosen to experimentally confirm the effect of the mutual coupling on the desired null pattern. A copper cylinder with a=127mm and h=2mm was used to mount the array of patches onto.

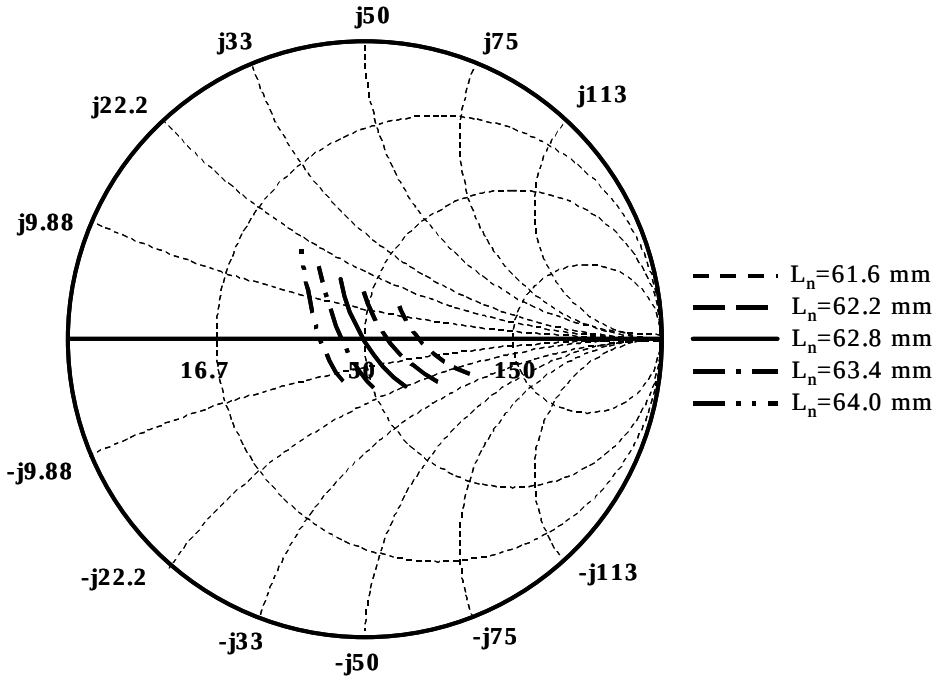

Figure 4.15: Input impedance of the patch antenna element for different L_n and 8.9mm $\leq y_n \leq$ 15.9mm. Figure 4.6 shows the configuration of the array where W_n is 65mm

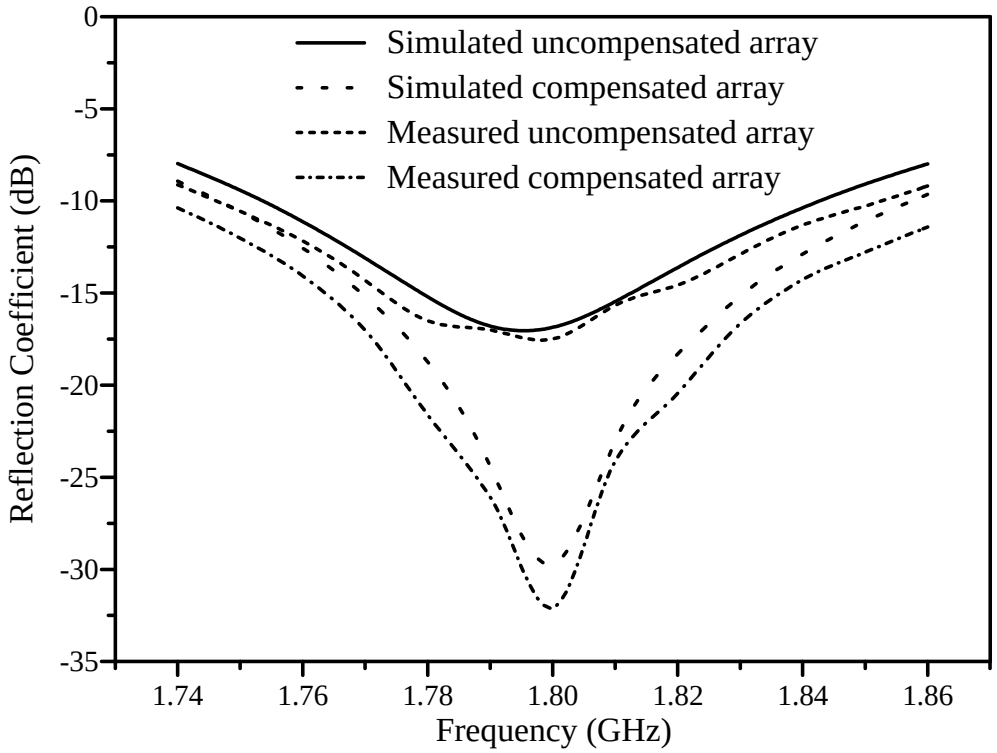

Figure 4.16: Simulated and measured reflection coefficients of the feeding network input ports for the original uncompensated and compensated arrays with $d = 0.65\lambda_0$

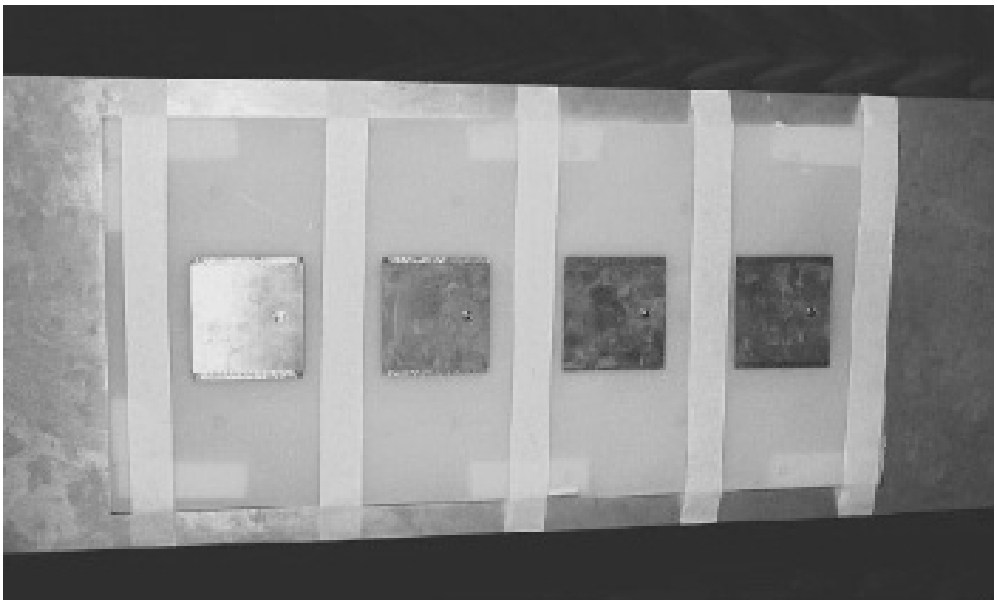

Figure 4.17: Top view of the original uncompensated linear microstrip patch antenna array

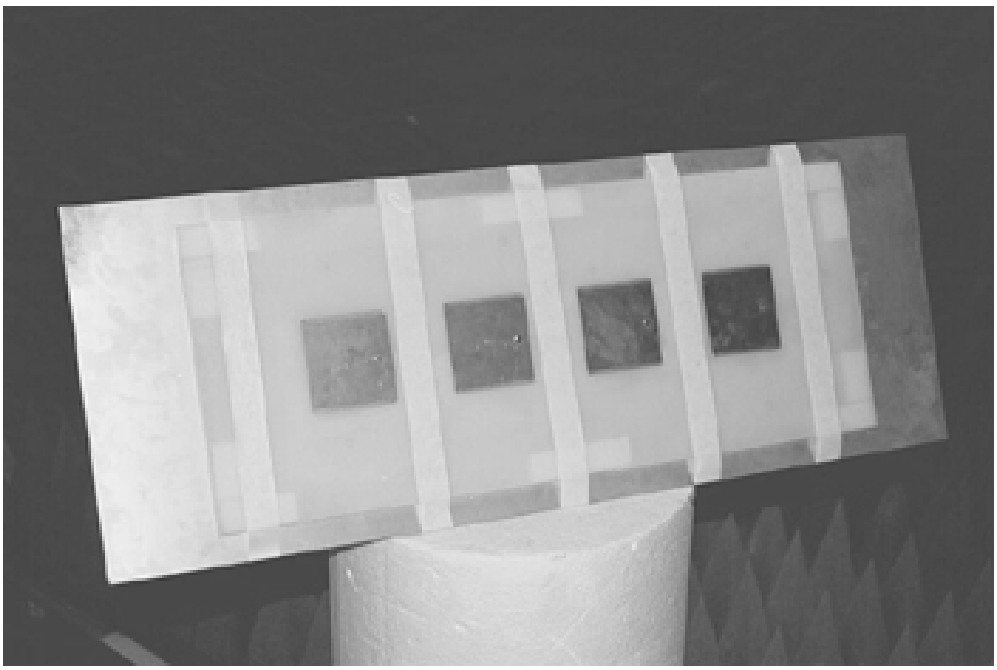

Figure 4.18: Top view of the compensated linear microstrip patch antenna array

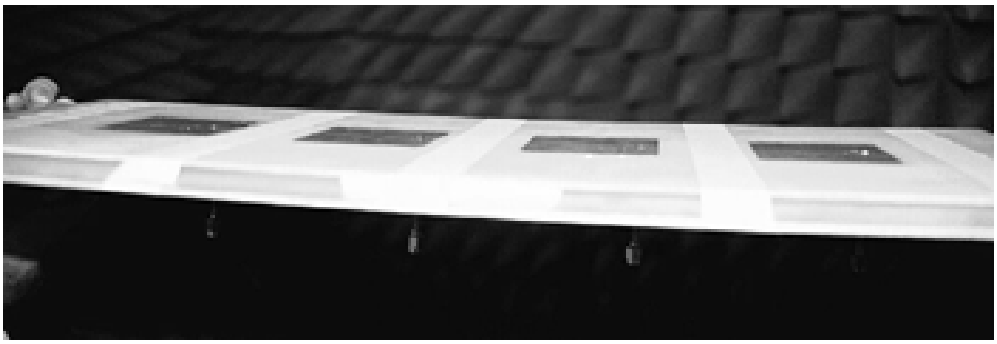

Figure 4.19: Side view of the compensated linear microstrip patch antenna array

The cylindrical patch antenna element was designed for a measured resonant frequency of 1.8 GHz, using the measured reflection coefficient data in paragraph 4.1 for the refinement of the design. The resulting dimensions were L=73.6 mm and W=76 mm, with the feed position at 16.6 mm from the centre of the patch in the z-direction. The resonant frequency and reflection coefficient, obtained from the simulation of the patch element with the FDTD software, were 1.727 GHz and -32.8 dB, respectively.

The cylindrical array was manufactured by etching the patch element array onto the thin layer of FR4 and wrapping it around the cylinder. The 5mm air gap was established by using 5mm polystyrene strips which were also wrapped around the cylinder. To excite the patch elements individually, each element was provided with a probe feed and a coaxial connector.

When the radiation pattern measurements were performed for the first set-up, significant differences were found between the active element patterns. This was due to the slight oval shape of the cylinder. Two PVC discs were then inserted at the bottom and top of the cylinder to ensure that the cylinder maintains a circular shape. The bottom PVC disc also provided the capability for mounting the cylinder on a post and for rotating it around its centre. Figures 4.20 and 4.21 provide the side and top view of the manufactured array, respectively.

The radiation pattern measurement was done in a compact measurement range. The active element pattern was measured for each element by exciting the particular element and terminating the feeds of the rest of the elements with 50Ω loads. The S-matrix of the array was measured using a network analyser in a measurement room partially filled with absorbing material. All measurements were done at 1.8 GHz.

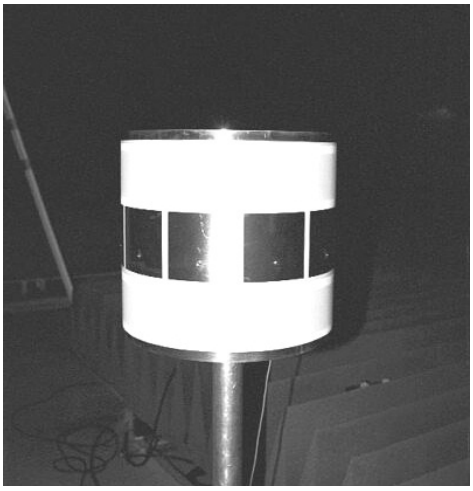

Figure 4.20: Side view of axially polarised microstrip patch array

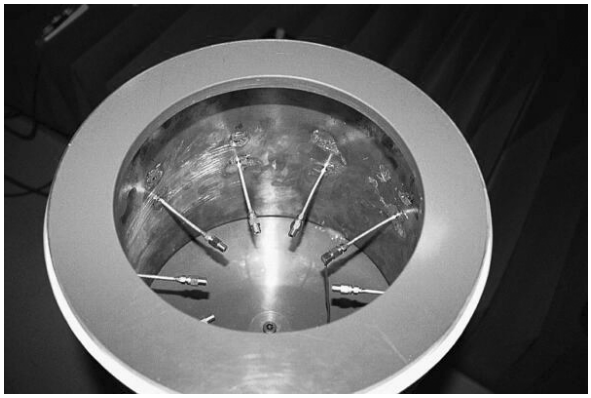

Figure 4.21: Top view of axially polarised microstrip patch array

Without including mutual coupling, the set of excitations for forming a -20 dB null at 180° in an otherwise omni-directional pattern was determined using the simulated radiation patterns of the isolated elements. The ripple was also constrained to 1 dB using the constrained optimisation method. The resulting unconstrained null width was found to be 20.2°. The mutual coupling was then included in the computation of the array pattern by using the simulated array imbedded element patterns and the active driving currents computed for this set of excitations using Equation 2.79. This analysis was repeated for the measured results by using the measured array imbedded element patterns and by computing active driving currents from the measured admittance matrix and the same set of excitations.

Figure 4.22 shows the resulting array patterns for the simulated and measured array

characteristics. The most significant changes in the array radiation pattern when the mutual coupling is included in the analyses, are the decrease in the null depth and the increase in the null width. For the simulated characteristics, the null depth decreased by 5.2 dB, while the null width increased by 3.7°. The null depth decreased by 3.4 dB and the null width increased by 2.9° for the measured array characteristics. The differences between the measured and simulated results are partially caused by the manufacturing tolerances. The input impedances of the antenna elements are sensitive to small variations in the height of the air layer underneath the patch. Any skewness in the probe feed of the patch antenna will also cause the input impedance and the array imbedded element pattern to differ from the simulated results. The differences between the measured and simulated results discussed in paragraph 4.1, also contribute the discrepancies between the simulated and measured results.

For this axially polarised cylindrical array, the length and feed positions of the antenna elements to compensate for the mutual coupling, were found. The look-up table of self-impedances was populated using simulation results. The mutual impedances was assumed to vary little for small changes in the patch lengths and feed positions and was kept constant in the optimisation algorithm. The resulting lengths and feed positions are listed in Table 4.11.

To study the resulting array pattern after the mutual coupling compensation, the cylindrical array was simulated with the modified patch elements. The simulations were done over the bandwidth (for VSWR ≤ 2) of the isolated patch element at 1.696, 1.727 and 1.760 GHz. Figure 4.23 compares the the resulting null pattern before and after the modification of the dimensions of the antenna elements. The resulting ripple was 1.31 dB, while the null depth and null width were -19.5 dB and 20.6°, respectively. To be practical, the lengths and feed positions of the patch elements were only incremented or decremented in steps of 0.1mm. The driving impedances of the patch elements were thus not adjusted to be exactly 50Ω. Small changes in the mutual coupling between the modified antenna elements also contributed to the higher than expected ripple. The null width and null depth compared well to the null width (20.2°) and null depth (-20 dB) when mutual coupling was not included in the analysis.

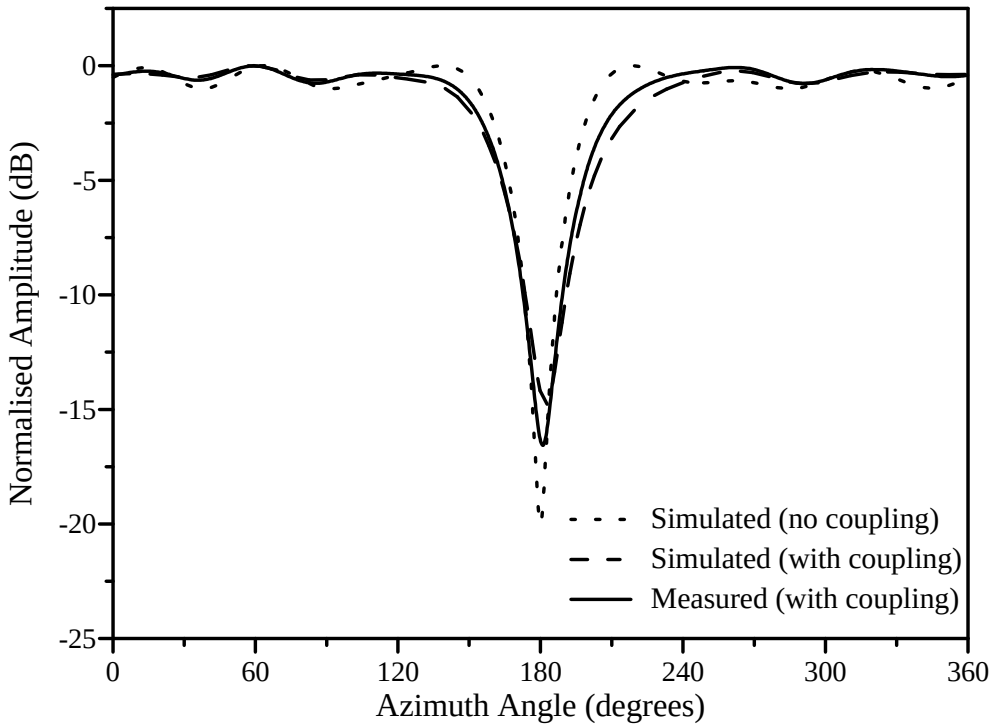

Figure 4.22: Comparison of the resulting null patterns for the simulated and measured array imbedded element patterns and array impedance matrices

Table 4.11: Lengths and feed positions needed to correct the active driving impedances of the axially polarised patch array

Element	**Length (mm)**	**Feed-position from centre (mm)**
1	73.2	17.2
2	73.2	17.2
3	73.4	18.6
4	73.6	16.6
5	72.6	15.0
6	74.0	19.4
7	73.2	16.4
8	73.8	18.9
9	73.0	17.0
10	73.6	18.0

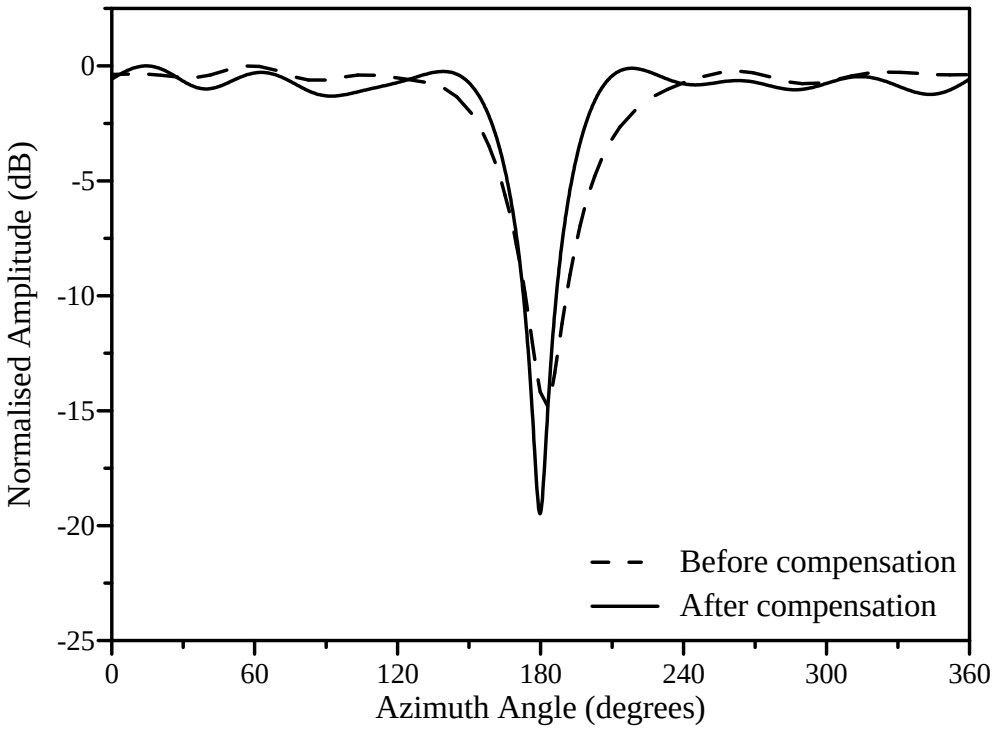

Figure 4.23: Comparison of the resulting null patterns, before and after mutual coupling compensation at 1.727 GHz

Figures 4.24 and 4.25 compare the null patterns before and after compensation at 1.696 and 1.76 GHz, respectively. Table 4.12 compares the characteristics of the null patterns for 1.696, 1.727 and 1.76 GHz before and after the compensation for the mutual coupling. After the coupling compensation technique was applied, the ripple increased by 0.48 and 0.4 dB at 1.696 and 1.76 GHz, respectively. In comparison, the ripple decreased by 0.19 dB and increased by 0.68 dB before the compensation at 1.696 and 1.76 GHz, respectively.

For this axially polarised patch array, the compensation thus limited the increase of the ripple at the higher frequency, but lead to more ripple change at the lower frequency. The ripple at 1.696 and 1.76 GHz, however, only differed by 0.08 dB. The null width and null depth had values close to the those of the desired pattern and changed little over the bandwidth. The null positions were also improved by the compensation technique.

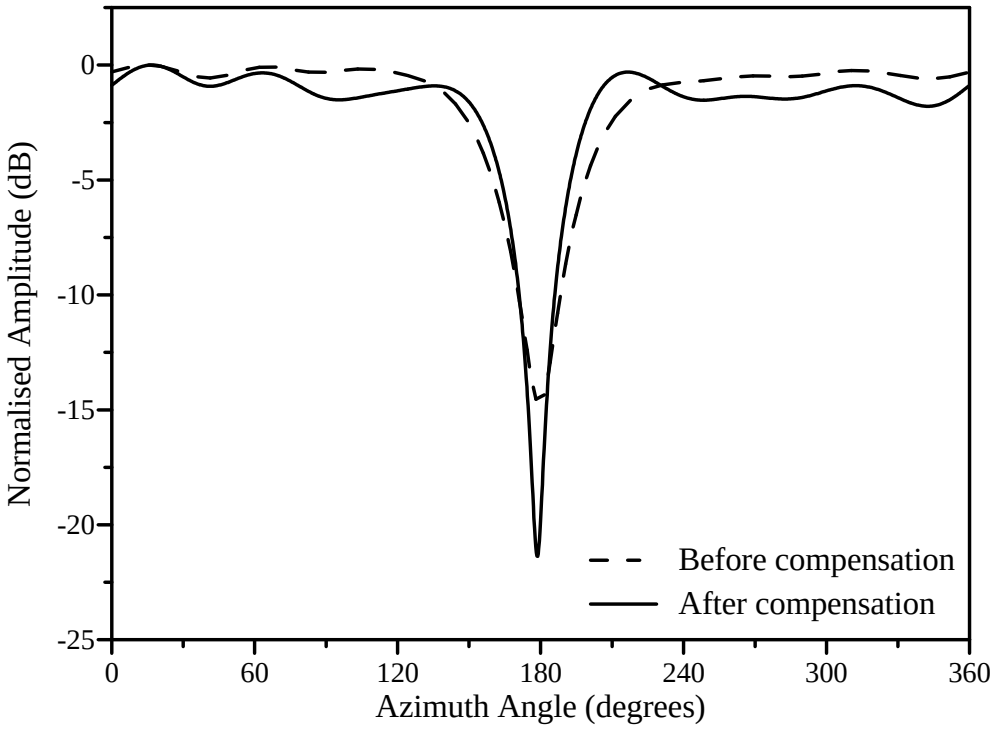

Figure 4.24: Comparison of the resulting null patterns, before and after mutual coupling compensation at 1.696 GHz

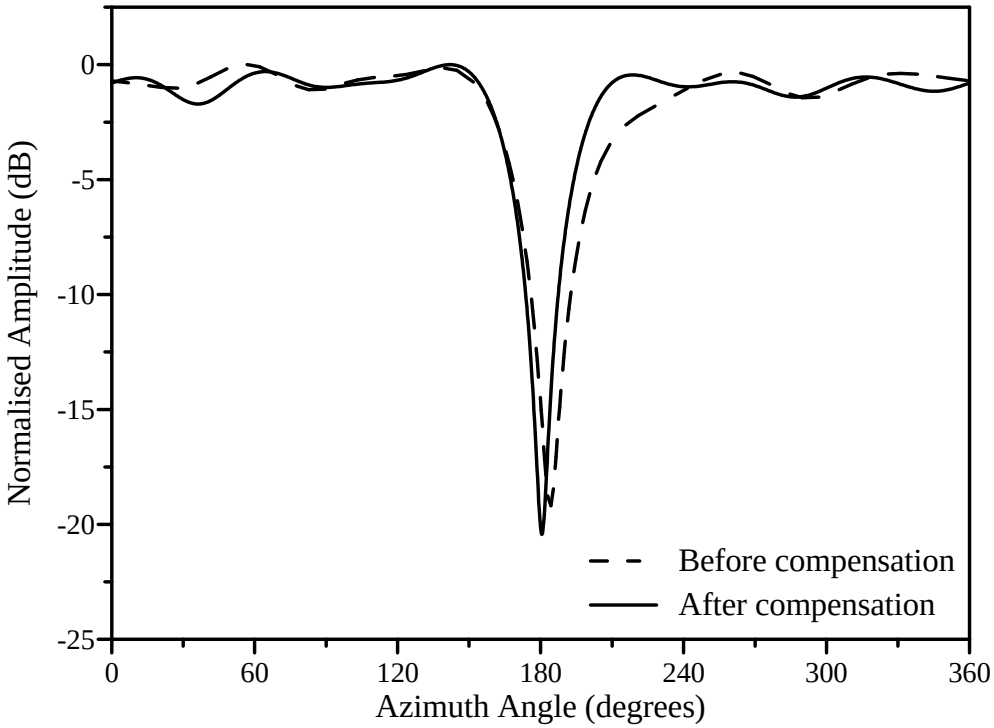

Figure 4.25: Comparison of the resulting null patterns, before and after mutual coupling compensation at 1.760 GHz

Table 4.12: Comparison of null pattern characteristics before and after compensation for the mutual coupling

Frequency (GHz)	**Before compensation**			**After compensation**		
	Ripple (dB)	**Null depth (dB)**	**Null width (°)**	**Ripple (dB)**	**Null depth (dB)**	**Null width (°)**
1.696	0.59	14.8	28.7	1.79	21.4	22.1
1.727	0.78	14.8	28.2	1.31	19.5	20.6
1.760	1.46	19.2	25.3	1.71	20.4	20.2

4.5 Summary

If the resulting element excitations obtained from the null synthesis techniques in the previous chapter, are applied to the cylindrical patch array, the resulting pattern will differ from the desired pattern. This is mainly due to the distortion of the excitations by the mutual coupling between the elements in an array [72, 73].

Before the effect of the mutual coupling on a cylindrical microstrip patch array was investigated, the cylindrical microstrip patch element was designed. A commercial electromagnetic software package applying the Finite Difference Time Domain (FDTD) method [101], was used to obtain simulated results. The approximations used in the simulation of a cylindrical patch antenna were discussed and the effects of these approximations were studied by comparing both simulated and measured results. The investigation was done for axially and circumferentially polarised patch antenna elements. The resulting reflection coefficient characteristics differed slightly from the desired characteristics. The measured shift in the resonant frequency and change in the input impedance could be applied to refine the design of the patch element. For both polarisations, the simulated and measured element radiation patterns compared well within the area of the main beam and differed slightly for the rest of the radiation pattern.

Firstly, the extent to which the mutual coupling affected the bandwidth of a narrowband linear microstrip arrays, was studied. This investigation was conducted in order

to study the improvement in the bandwidth due to the use of a mutual coupling compensation technique. The study was conducted for a four element linear microstrip patch array with a cooperate feed network and the results were compared for different inter-element spacing and polarisations. It was seen that both the minimum of the reflection coefficient at the input port of the feeding network and the resonant frequency are influenced by the mutual coupling. For a horizontally polarised array with E-plane coupling and an inter-element spacing of $0.5\lambda_0$, the resonant frequency was shifted by 2.8%, which is close to the bandwidth of an isolated element. As expected, the effect of the mutual coupling on the bandwidth and resonant frequency was less for larger inter-element spacing. The resonant frequency and bandwidth was less affected for a vertically polarised array with H-plane coupling due to the smaller magnitude of this coupling. The reflection coefficient, however, was -16.5 dB for the smallest inter-element spacing.

It was evident that the characteristics of narrowband arrays were affected by the mutual coupling. A high coupling factor could alter the resonant frequency to such an extent that the active bandwidth falls outside the desired bandwidth of the array. To match the desired and active characteristics of the linear patch arrays, a mutual coupling compensation technique was needed.

During null synthesis, erroneous excitations due to the mutual coupling lead to null filling and null position errors [53, 74]. The nulls introduced in the beam patterns of linear monopole arrays were found to be shifted or filled due to the mutual coupling [74]. Abele [53] studied the effect of the mutual coupling on the null pattern of a cylindrical dipole array and concluded that the coupling needed to be compensated for to prevent distortion of the null pattern characteristics. In this chapter, an investigation into the extent to which the mutual coupling has an influence on the null pattern of a cylindrical microstrip patch array was done.

The coupling in an array has an effect on the array imbedded radiation pattern of the element. Heberling et al. [17, 19] found that the main beam in the array imbedded radiation pattern is broadened by the coupling. In this chapter, the effects of the coupling on the array imbedded element radiation pattern were also investigated for an axially polarised patch array with N =10 and $d_\phi = 0.5\lambda_0$. Both simulated and measured results indicated a broadening in the main beam of the element pattern due to the coupling. It is thus important to use the array imbedded element pattern when

determining the excitation coefficients for a specified array radiation pattern in order to prevent distortion of the resulting array pattern.

For both polarisations, a cylindrical patch array was simulated to study the influence of the mutual coupling on an omnidirectional radiation pattern with a single null. It was seen that the gain ripple in the omni-region, as well as the null depth and width changed due to the coupling. The null position was also influenced. The null positions and null widths were more significantly affected for the circumferential polarisation, than for the axial polarisation. The radiation patterns of axially polarised arrays were less affected by the coupling for small inter-element spacing. This is due to the smaller coupling between the axially polarised patches. For large inter-element spacing, the element excitations were more sensitive to mutual coupling for both polarisations. From this study it was seen that in order to obtain the desired null patterns, the mutual coupling in the cylindrical patch arrays needed to be compensated for.

Given a required set of excitations, the geometries of the array elements can be varied to provide matched and equal driving impedances for all the antenna elements. Yang *et al* [86] proposed a mutual coupling compensation technique to obtain the desired bandwidth and voltage standing wave ratio (VSWR) at the resonant frequency for an electromagnetically coupled (EMC) dipole antenna array. For a given set of excitation voltages, the dipole lengths and dipole offsets from the microstrip feed line were altered to obtain the prescribed driving admittances seen by the feed lines. As a result, a good comparison was also found between the desired and measured radiation patterns. Chen [88, 89] varied the lengths and radii of the dipoles in linear and planar arrays to obtain the desired radiation patterns as well as equal driving impedances for the dipoles.

In this chapter, the above compensation technique was applied to linear and cylindrical microstrip patch antenna arrays. For the patch antenna elements the lengths and feed positions were varied to adjust the self and mutual impedances. The widths and heights of the patch antennae, were kept constant to reduce the dimensionality of the variable space of self-impedances. The self and mutual impedances were computed for linear spaced values of lengths and feed positions and were placed in lookup tables. These tables were used by a least squares optimisation algorithm which interpolated between the impedance values and determined the lengths and feed positions at which the driving impedances of all the patches were equal to 50Ω.

The lengths and feed positions of the cylindrical patch elements were varied to obtain matched driving impedances for a given set of excitations. The computed set of excitations was for a single null in an otherwise omnidirectional array pattern. For an axially polarised array, suitable lengths and feed-positions could be found within the available variable space for all the inter-elements spacing that was studied and null depths up to 40 dB. On the other hand, the higher mutual coupling in the circumferentially polarised patch arrays restricted the null depth for which the coupling could be compensated for using the described technique. For the smallest inter-element spacing studied ($d_\phi = 0.5\lambda_0$), the maximum realisable null depth was found to be 10 dB. As the inter-element spacing was increased, the possible null depth could be increased while still being able to correct the driving impedances by finding suitable lengths and feed positions within the available variable space.

To confirm the proposed coupling compensation experimentally, a four element linear microstrip patch array with E-plane coupling was used. The lookup tables were set up using a commercial electromagnetic software package which utilises the method of moments. The optimisation algorithm was then used to obtain the required lengths and feed positions to correct the driving impedances. A linear array was manufactured with the resulting dimensions to verify the improvement in the reflection coefficient characteristics at the input port of the array. Good agreement was obtained between the simulated and measured reflection coefficients. The compensation technique improved the resonant frequency to be within 0.1% of the desired frequency and the measured bandwidth was increased significantly.

An axially polarised cylindrical patch array was also designed and manufactured to confirm the effects of the mutual coupling on a desired null pattern. The active element patterns as well as the S-matrix were measured. The resulting pattern for the desired set of element excitations was determined using the measurement data and compared to the pattern obtained using simulated data. There was little difference between the null depths and null widths of the two patterns.

For the manufactured cylindrical patch array, the lengths and feed positions of the antenna elements were varied to correct the driving impedances for the desired set of element excitations. To study the resulting array null pattern after the mutual coupling compensation, the cylindrical array was simulated with the modified patch elements over the bandwidth of the isolated patch element. The resulting null patterns were

also compared to the null patterns before the mutual coupling compensation. Over the studied frequency band, the resulting null widths and depths compared well to the null widths and depths of the desired null pattern and varied little. The null positions were also improved over the whole frequency band. When the results at the centre frequency and the lowest frequency were compared, the ripple increased by 0.48 dB. Towards the highest frequency, the ripple increase was limited to 0.4 dB. The resulting gain ripple at the lowest and highest frequency differed by only 0.08 dB for the compensated array. This was an improvement on the ripple variation of 0.87 dB over the bandwidth for the uncompensated array.

For the cylindrical microstrip patch array used in the test case, the effect of the mutual coupling on the null pattern was not severe. If the changes in the null pattern characteristics are not severe and can be tolerated by the system which the antenna is integral to, the mutual coupling compensation is not needed. This can be an advantage, especially when the array is used in an adaptive system.